American Mineralogist, Volume 80, pages 1031–1040, 1995

# Zirconosilicate phase relations in the Strange Lake (Lac Brisson) pluton, Quebec-Labrador, Canada

STEFANO SALVI,* ANTHONY E. WILLIAMS-JONES
Department of Earth and Planetary Sciences, McGill University, 3450 University Street, Montreal, Quebec H3A 2A7, Canada

## ABSTRACT

Petrographic observations of subsolvus granites at Strange Lake indicate that the sodium zirconosilicate elpidite crystallized under magmatic conditions, but that the calcium zirconosilicates armstrongite and gittinsite are secondary. This interpretation is consistent with the extensive solid solution displayed by elpidite and the restricted compositions of armstrongite and gittinsite. Both calcium zirconosilicate minerals show textural evidence of having replaced elpidite, and in the case of gittinsite, with major volume loss. In the near-surface environment, gittinsite plus quartz fill the volume formerly occupied by elpidite. At greater depth, gittinsite and armstrongite partially replaced elpidite but are not accompanied by quartz, and abundant pore space is observed where gittinsite is the principal secondary phase. Below 70 m elpidite is generally unaltered. Replacement of elpidite by armstrongite is interpreted to have been a result of the cation-exchange reaction

$$\underset{\text{elpidite}}{Na_2ZrSi_6O_{15}\cdot 3H_2O} + Ca^{2+} = \underset{\text{armstrongite}}{CaZrSi_6O_{15}\cdot 3H_2O} + 2Na^+$$

in which volume is nearly conserved, and replacement by gittinsite is thought to have resulted from the reaction

$$\underset{\text{elpidite}}{Na_2ZrSi_6O_{15}\cdot 3H_2O} + Ca^{2+} + 5H_2O = \underset{\text{gittinsite}}{CaZrSi_2O_7} + 2Na^+ + 4H_4SiO_4^0$$

which is accompanied by a 65% volume reduction.

An alteration model is proposed in which external Ca-rich, quartz-undersaturated fluids dissolved elpidite and replaced it with gittinsite, where $a_{H_4SiO_4^0}$ was buffered mainly by the fluid (high water-rock ratio), and with armstrongite plus gittinsite, or armstrongite alone, where $a_{H_4SiO_4^0}$ was buffered to higher values by the rock (low water-rock ratio). The formation of gittinsite created extensive pore space that was subsequently filled, in the upper part of the pluton, when the fluid became saturated with quartz as its temperature decreased during the final stages of alteration.

## INTRODUCTION

In most igneous rocks, Zr is an incompatible trace element present in amounts ranging from <10 to several hundred parts per million and is accommodated as the accessory mineral zircon. However, in peralkaline igneous rocks its concentration is commonly orders of magnitude higher and may be locally sufficient to constitute a potentially exploitable deposit (e.g., Ilímaussaq: Gerasimovsky, 1969; Lovozero: Kogarko, 1990; Strange Lake: Miller, 1986; Kipawa: Allan, 1992; and Thor Lake: Trueman et al., 1988). The Zr mineralogy of peralkaline rocks is also unusual. Although most peralkaline rocks contain some zircon, the bulk of the Zr commonly occurs as one or more of a large family of alkali and alkaline-earth zirconosilicate minerals. The most important of these are catapleiite ($Na_2ZrSi_3O_9\cdot 2H_2O$), dalyite ($K_2ZrSi_6O_{15}$), elpidite ($Na_2ZrSi_6O_{15}\cdot 3H_2O$), eudialyte [$Na_4(Ca,Ce)_2(Fe^{2+},Mn,Y)ZrSi_8O_{22}(OH,Cl)_2$], vlasovite ($Na_2ZrSi_4O_{11}$), and wadeite ($K_2ZrSi_3O_9$), any of which may be the principal zirconosilicate mineral in a particular setting, e.g., eudialyte at Lovozero (Vlasov et al., 1966), catapleiite at Mont-Saint-Hilaire (Horváth and Gault, 1990), and vlasovite on Ascension Island (Fleet and Cann, 1967).

Little is known about the factors controlling the distribution of zirconosilicate minerals, and there is little documentation of their parageneses. The only reversed experimental study that provides data on their stability at geologically meaningful conditions is that of Currie and Zaleski (1985) on the dehydration reaction of elpidite to vlasovite and quartz. Marr and Wood (1992) constructed

* Present address: Laboratoire de Géochimie-CNRS, Université Paul Sabatier, 38 rue des Trente-Six Ponts, Toulouse F-31400, France.

0003–004X/94/0910–1031$02.00

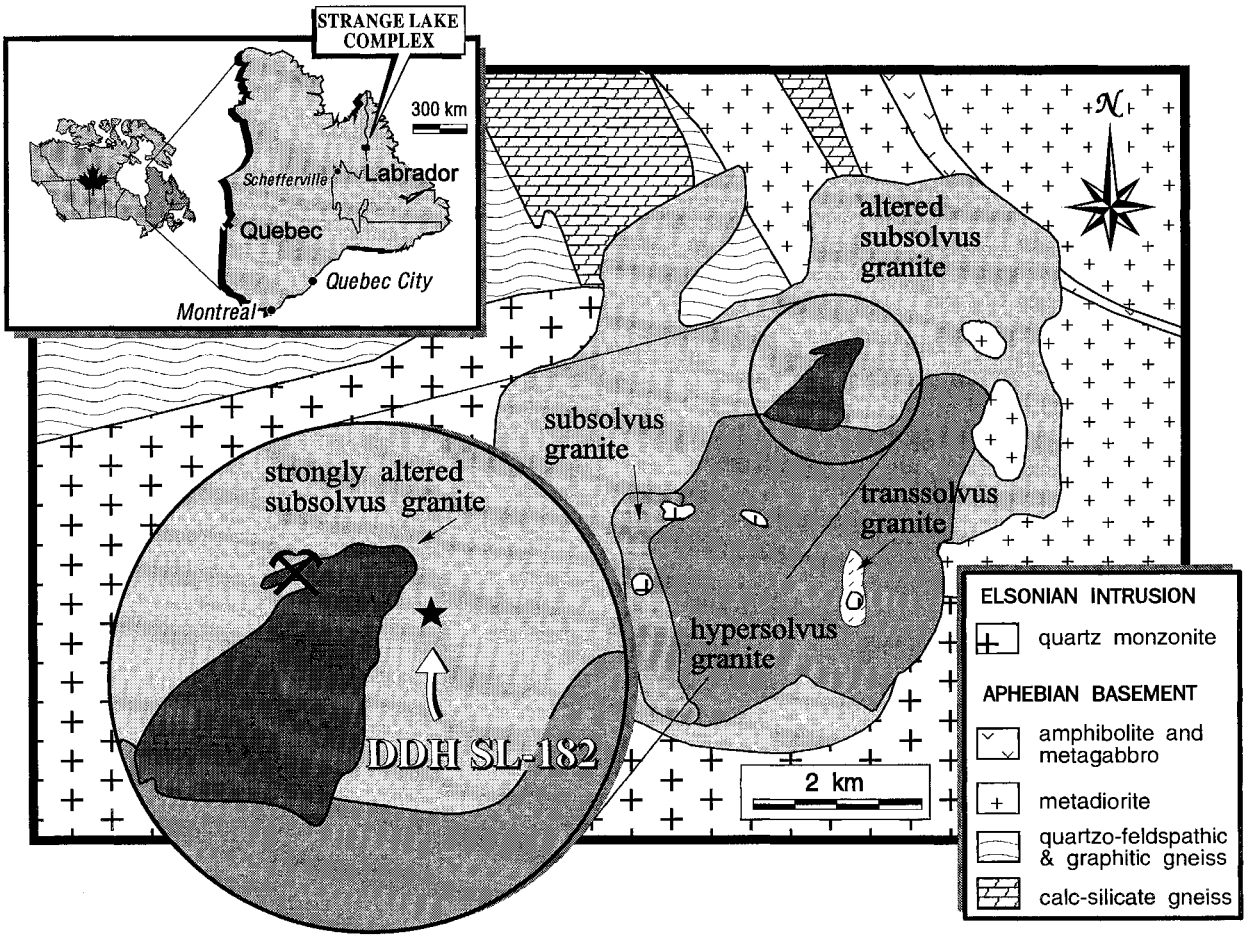


Fig. 1. Location and simplified geological map of the Strange Lake pluton (modified after Salvi and Williams-Jones, 1992).

theoretical *P-T* diagrams for sodium and calcium zirconosilicate minerals using the results of Currie and Zaleski (1985), molar volume data, and the few constraints available from natural systems. Further advances in our understanding of Zr mineral petrogenesis will require basic thermodynamic data for the major phases and careful documentation of field occurrences. The latter is the objective of the present contribution.

In the Strange Lake pluton, Zr occurs mainly in the form of the zirconosilicate minerals elpidite, armstrongite ($CaZrSi_6O_{15} \cdot 3H_2O$), and gittinsite ($CaZrSi_2O_7$). These minerals vary greatly in their relative proportions, and, locally, any one of them may be the principal or sole Zr phase. The highest concentrations of Zr are in rocks containing only gittinsite. Salvi and Williams-Jones (1990) observed that gittinsite plus quartz form pseudomorphs after an unidentified phase; on the basis of the morphology of the pseudomorphs and on fluid-inclusion evidence, they suggested that a Ca-bearing fluid at ~200 °C caused the metasomatic transformation of the sodium zirconosilicate elpidite to gittinsite + quartz. Birkett et al. (1992) subsequently proposed that gittinsite replaced the calcium zirconosilicate armstrongite, which they claimed occurs both as phenocrysts and as a replacement of elpidite.

We reexamine the genesis of elpidite, armstrongite, and gittinsite at Strange Lake, in light of textural and mineral chemical data collected from a representative diamond-drill hole located near the zone of economic interest. These data, in conjunction with mineral stability relationships and published fluid-inclusion data (Salvi and Williams-Jones, 1990), support a model involving low-temperature metasomatic replacement of elpidite by armstrongite and gittinsite.

## Geological setting

The Strange Lake pluton (1189 ± 32 Ma, Pillet et al., 1989), located in the eastern Rae province of the Canadian Shield, is a peralkaline granite that intruded Aphebian metamorphic rocks (1.8 Ga) and an Elsonian quartz monzonite (1.4 Ga) (Fig. 1). The intrusion is a subvertical, cylindrical body approximately 6 km in diameter and represents the latest tectonic event in the area. Large roof pendants are commonly observed (Fig. 1), suggesting that

the present erosional surface is close to the apical part of the pluton. On the basis of its peralkalinity, mode of emplacement, and age, the pluton may represent the Labrador extension of the Gardar anorogenic igneous event (Currie, 1985; Pillet et al., 1989).

Several concentric intrusive pulses of peralkaline granite formed the Strange Lake pluton, represented by hypersolvus granite, transsolvus granite, and more evolved, volatile-saturated subsolvus granites (Nassif and Martin, 1991) (Fig. 1). All phases are F-rich and contain primary fluorite. They are mainly leucocratic, fine to medium grained, and quartz saturated. Pegmatites are common and concentrated mainly in the subsolvus granite. An outwardly dipping ring fracture, marked by a heterogeneous breccia in a fluorite-filled matrix, surrounds the pluton.

The hypersolvus granite consists largely of phenocrysts of quartz and perthite, and interstitial arfvedsonite, whereas the subsolvus granite contains two alkali feldspars (albite and microcline), and arfvedsonite commonly occurs as phenocrysts. Transsolvus granite is transitional to the two other types of granite, i.e., it contains perthite phenocrysts in addition to albite and microcline. Arfvedsonite in this unit occurs predominantly as fine-grained anhedra, imparting a melanocratic appearance to the rock. The hypersolvus granite contains up to 5% of zirconosilicate minerals, and the subsolvus granite and pegmatites contain up to 30% of these minerals. Elpidite is the principal Zr mineral in the hypersolvus granite, whereas elpidite, armstrongite, and gittinsite are the dominant Zr minerals in the subsolvus granite and pegmatites. Less common zirconosilicates at Strange Lake include catapleiite, calcium catapleiite, dalyite, hilairite ($Na_2ZrSi_3O_9 \cdot 3H_2O$), vlasovite, and zircon (cf. Birkett et al., 1992).

Subsolvus granites commonly display hematitic alteration and, where altered, have higher Zr contents than fresh hypersolvus or subsolvus granites (Fig. 2). Hematization was associated with the development of secondary high-field-strength element (HFSE) minerals, many of which are Ca-bearing. Some of the most intense hematization is in the center of the complex, where a subeconomic ore zone has been delineated containing some 30 million tonnes grading 3.25% $ZrO_2$, 1.3% REE oxides, 0.66% $Y_2O_3$, 0.56% $Nb_2O_5$, and 0.12% BeO (Iron Ore Company of Canada, unpublished data). These granites have lower alkali contents, higher $Fe^{3+}/Fe^{2+}$, and higher Ca contents than fresh or less-altered subsolvus rocks (Miller, 1986; Salvi and Williams-Jones, 1990; Boily and Williams-Jones, 1994). Salvi and Williams-Jones (1990) provided fluid-inclusion evidence of the interaction of ore-zone rocks with a low-temperature, $CaCl_2$-dominated brine. The high $\delta^{18}O$ of these rocks suggests that the fluid was externally derived (cf. Boily and Williams-Jones, 1994). A second episode of alteration is represented by the replacement of arfvedsonite by aegirine. This event is not well constrained temporally but has been shown to be limited spatially to the subsolvus granite and is thought to represent an earlier, high-temperature event (Salvi and Williams-Jones, 1992). Significantly, this alteration is most strongly developed as halos around pegmatites that contain primary high-temperature fluid inclusions rich in NaCl and without detectable Ca.

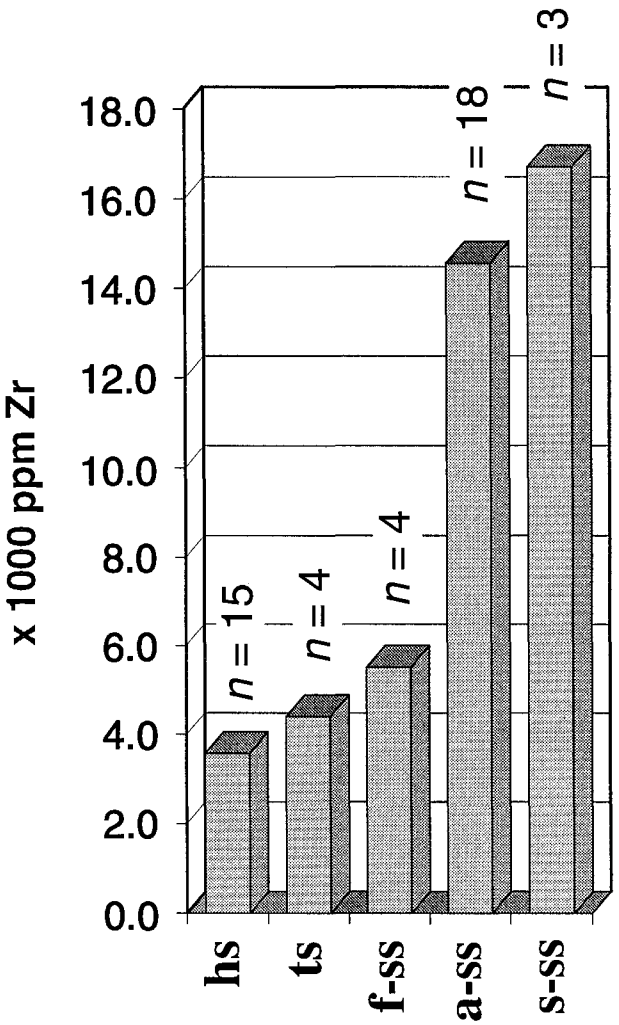


Fig. 2. A histogram showing the average whole-rock content of Zr in the principal varieties of granite at Strange Lake. Abbreviations: hs = hypersolvus, ts = transsolvus, f-ss = fresh subsolvus, a-ss = altered subsolvus, and s-ss = strongly altered subsolvus. Standard deviations are 1.9, 2.4, 1.3, 2.3, and 0.3 × 1000 ppm, respectively.

## Geology of DDH SL-182

The diamond-drill hole that is described in detail below is one of the deeper (88 m) of some 35 drill holes that were logged by the authors and is located approximately 700 m southeast of the main exploration trench (Fig. 1). This hole provides a representative cross section of the alteration and intersects several varieties of subsolvus granite, as well as several pegmatites (Fig. 3). All rock units contain one or more of the zirconosilicate minerals elpidite, armstrongite, and gittinsite.

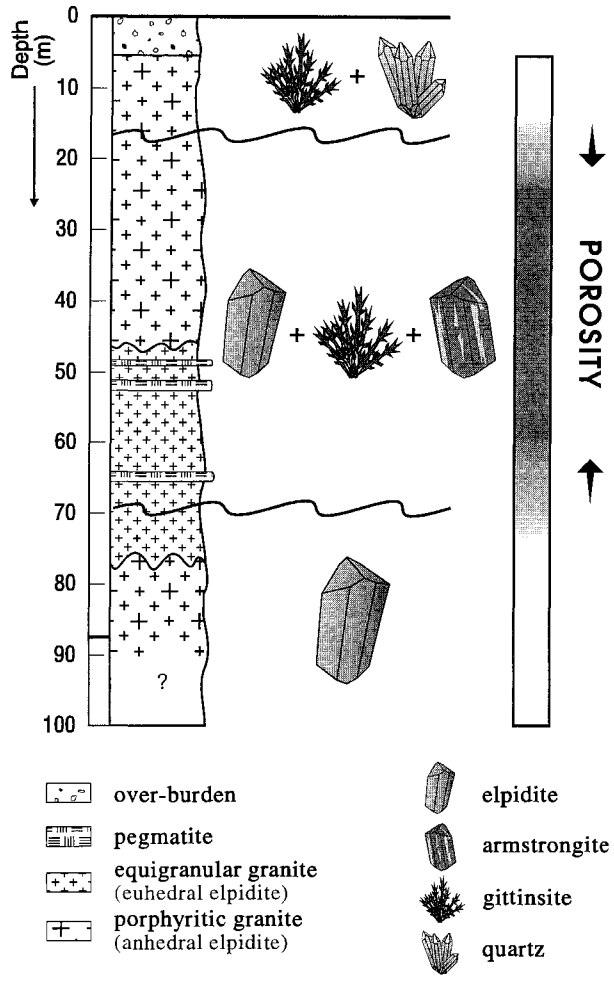


Fig. 3. A schematic representation of the geology, the zirconosilicate mineral habits and distribution, and the porosity profile of DDH SL-182. Darker shading corresponds to higher porosity.

The top half and final 13 m of the hole are composed of fine- to medium-grained porphyritic granite containing phenocrysts of arfvedsonite. This unit contains inclusions of transsolvus granite ranging from one to a few tens of centimeters in diameter and constituting 2–5% by volume of the rock.

In the central portion of the hole, the granite is also fine to medium grained but lacks arfvedsonite phenocrysts and transsolvus granite inclusions. Subhedral to euhedral aegirine occurs locally. The lower contact between this and the porphyritic granite is gradational over a few meters, with the proportion of arfvedsonite phenocrysts decreasing upwards and the zirconosilicates having two habits (see below). The upper contact is more abrupt, although lacking a chilled margin. This and the absence of other evidence of intrusive relationships suggest that these two main rock types were roughly coeval. The equigranular granite is intersected in other drill holes and is exposed in the trench, west of DDH SL-182. It can therefore be deduced that this unit forms a subhorizontal sheet a few tens of meters in thickness in the central portion of the pluton (cf. Miller, 1990; Birkett et al., 1992).

The granites are altered to varying degrees, except in the bottom 10 m of the hole where they are relatively fresh. Alteration is manifested as a replacement of arfvedsonite by aegirine ± hematite, replacements involving the zirconosilicates (see below), hematite staining (particularly near the top of the hole), red $Fe^{3+}$-activated cathodoluminescence of feldspars, appearance of secondary fluorite, and the development of extensive secondary porosity. The strongest replacement of arfvedsonite by aegirine is observed in and adjacent to several meterwide pegmatites that cut the equigranular granite.

## Distribution of zirconosilicate minerals in DDH SL-182

Euhedral elpidite occurs as doubly terminated orthorhombic prisms, with the typical boat shape also observed in rocks from Narssârssuk by Goldschmidt (1913). Euhedral armstrongite has a pseudo-orthorhombic habit indistinguishable from that of elpidite. All observed occurrences of armstrongite show polysynthetic twinning. Gittinsite occurs almost exclusively as narrow feathery crystals forming radiating aggregates.

Elpidite, armstrongite, and gittinsite have distinctly different distributions and modes of occurrence (Fig. 3). In the porphyritic granite at the bottom of the hole, elpidite is the principal zirconosilicate mineral, and its abundance ranges from a few percent to 20% of the rock by volume; armstrongite is absent, and gittinsite is rare. Elpidite occurs as anhedra up to 3 mm in diameter interstitial to feldspar and quartz grains (Fig. 4A) or as large aggregates of small grains (<0.1 mm in diameter) also distributed interstitially to the main rock-forming minerals (Fig. 4B).

Fig. 4. Photomicrographs of zirconosilicate mineral textures: (**A**) (74.9 m depth) anhedral crystal of elpidite (elp) and (**B**) aggregate of small elpidite crystals interstitial to quartz (qtz) and feldspar (feld); (**C**) (54.9 m) euhedral crystal of elpidite; (**D**) (53.0 m) partial replacement of elpidite by polysynthetically twinned armstrongite (arm); (**E**) (59.4 m) gittinsite (git) rosettes, accompanied by pore space, partly replacing large elpidite crystals; (**F**) (44.7 m) radiating gittinsite crystals attached to a string of secondary zircon spherules and growing in pore space adjacent to elpidite; (**G**) (13.5 m) aggregate of feathery gittinsite crystals plus quartz interstitial to quartz and feldspars; (**H**) (trench sample) gittinsite-quartz pseudomorph after a euhedral phase. Photos **A**, **B**, **C**, **D**, **E**, and **H** are in crossed polarized light; **F** and **G** in plain polarized light. Photos **A**, **B**, **C**, **E**, and **G** are 2 mm across; **D**, **F**, and **H** are 1 mm across. →

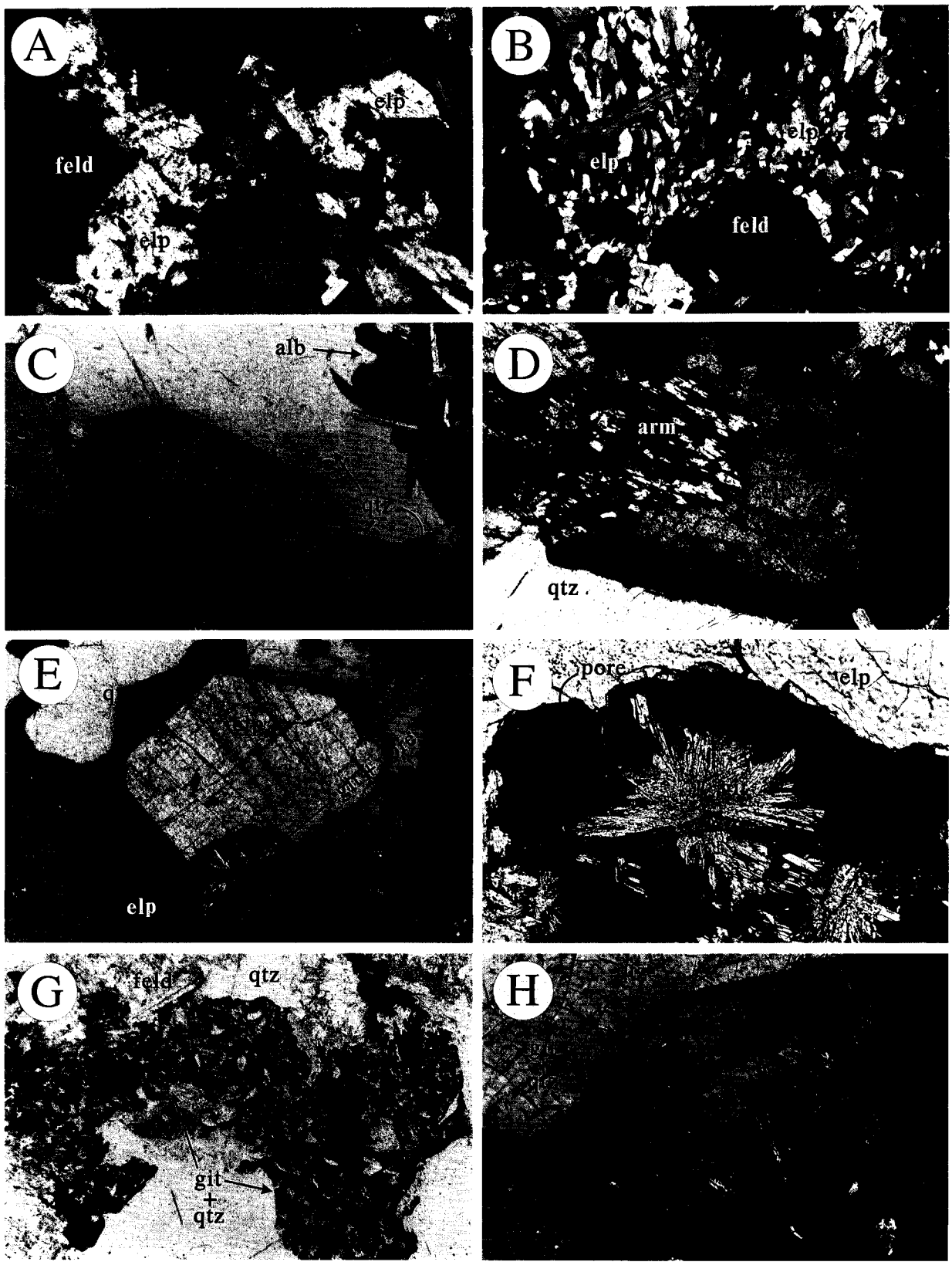
A
elp
feld
elp
B
elp
elp
feld
C
alb
D
arm
qtz
E
elp
F
pore
elp
G
feld
qtz
git
+
qtz
H

**TABLE 1.** Representative and average composition of zirconosilicates

| | Elpidite | | | | Averages | | |
|---|---|---|---|---|---|---|---|
| | Near end-member | | Ca-rich | | Elpidite $n = 46$ | Armstrongite $n = 14$ | Gittinsite $n = 20$ |
| $SiO_2$ | 62.0 | 63.5 | 63.2 | 63.6 | 62.9 | 63.4 | 41.9 |
| $TiO_2$ | n.d. | n.d. | 0.20 | n.d. | 0.27 | 0.16 | 0.17 |
| $ZrO_2$ | 19.0 | 18.9 | 17.9 | 16.2 | 17.1 | 19.2 | 36.9 |
| FeO* | n.d. | n.d. | n.d. | 0.29 | 0.07 | 0.07 | 0.43 |
| MgO | 0.60 | 0.32 | 0.75 | 0.54 | 0.44 | 0.09 | 0.23 |
| MnO | n.d. | n.d. | n.d. | n.d. | 0.07 | n.d. | 0.74 |
| CaO | 0.19 | n.d. | 1.42 | 2.43 | 0.92 | 10.0 | 17.7 |
| $Na_2O$ | 8.83 | 8.09 | 7.69 | 8.04 | 9.01 | n.d. | 0.13 |
| $K_2O$ | n.d. | n.d. | n.d. | n.d. | 0.21 | 0.23 | n.d. |
| $Nb_2O_5$ | n.d. | n.d. | n.d. | n.d. | 0.46 | 0.35 | 0.60 |
| $Ce_2O_3$ | n.d. | n.d. | n.d. | n.d. | n.d. | n.d. | 0.85 |
| $Nd_2O_3$ | 0.46 | n.d. | n.d. | n.d. | 0.13 | 0.10 | 0.21 |
| Total | 91.1 | 90.8 | 91.1 | 91.1 | 91.6 | 93.5 | 99.8 |

*Note:* n.d. = not detected. Analyses are reported in weight percent.
* Total Fe as FeO.

Elpidite is also the dominant zirconosilicate mineral in the equigranular granite (middle of the hole), but it forms euhedral crystals (Fig. 4C) up to 3 mm long, and its abundance varies between 15 and 25% of the rock by volume. Many elpidite crystals display varying degrees of rim and core replacement by armstrongite and gittinsite. The volume proportion of elpidite replaced by these minerals averages 15–20% and increases upwards. Where replacement involved armstrongite alone, volume was conserved (Fig. 4D). However, elpidite crystals replaced by gittinsite or by armstrongite + gittinsite all contain pore space (Fig. 4E and 4F). Although armstrongite can be found in contact with both elpidite and gittinsite, the latter minerals rarely occur in contact with each other. In the transitional zone between the two granites, both interstitial and euhedral habits of elpidite are observed.

Farther up the hole (15–46 m), in porphyritic granite, elpidite has a habit similar to that of elpidite in the deepest part of the hole. However, in this interval it experienced extensive dissolution, leaving behind pore space (up to 10% of the rock) and calcium zirconosilicates, largely gittinsite (Fig. 4F). In cases where an entire pocket of elpidite was replaced, the proportions of gittinsite and pore space are about 40 and 60%, respectively, of the precursor elpidite. Armstrongite is a minor phase and replaced either cores or rims of elpidite crystals. Replacement of elpidite is more extensive toward the top of the interval.

In the top 10–15 m of drill core, gittinsite is the sole zirconosilicate mineral. It forms feathery radiating crystals up to 0.5 mm in length embedded in tiny anhedral quartz grains. Gittinsite and quartz form coherent aggregates in the groundmass, interstitial to other minerals (Fig. 4G). The sizes, shapes, and sharp boundaries of these aggregates suggest that they fill interstitial volumes formerly occupied by crystals of elpidite. In this interval, gittinsite makes up from 5 to 20% of the rock by volume. The granite is almost free of porosity and displays a patchy red coloration because of fine-grained hematite in the gittinsite-quartz aggregates.

Rocks from the exploration trench, similar in texture and mineral assemblage to the equigranular granite in DDH SL-182, as well as equigranular granite intersected at high levels by other drill holes, also contain aggregates of gittinsite plus quartz and lack porosity. However, in contrast to the upper part of hole DDH SL-182, these aggregates form pseudomorphs after a euhedral phase (Fig. 4H), which we interpret to be elpidite on the basis of the occurrence of elpidite crystals with similar morphology in equigranular granite in DDH SL-182. The volume proportions of gittinsite and quartz in the pseudomorphs, whether after euhedral or interstitial elpidite, vary from 40 to 70% and 30 to 60%, respectively. Interestingly, the gittinsite-quartz pseudomorphs in both equigranular and porphyritic granite occur where hematite alteration is most intense.

## Geochemistry

Electron microprobe analyses were performed with a Cameca CAMEBAX equipped with an EDS detector (NORAN high-purity Ge detector, NORVAR window). Analyses were conducted in EDS mode to permit use of a low beam current (15 kV, 0.6 nA current, and 2000–3500 counts), to minimize the volatility of light elements such as Na (light-element volatility is the major source of error in zirconosilicate mineral analysis; see Bonin, 1988; Birkett et al., 1992). Where possible, the beam was defocused to a diameter of 5 $\mu$m to minimize further light-element volatility. Data reduction was performed with the PROZA version of the $\phi(\rho,Z)$ correction routine using internal standards (Bastin and Heijligers, 1991).

Compositions of each zirconosilicate are listed in Table 1 and are plotted as atomic proportions of Na, Ca, and Zr/(Zr + Si) in Figure 5. The data indicate that elpidite contains up to 37 mol% of armstrongite in solid solution. By contrast, most of the gittinsite and armstrongite samples have compositions very close to those of the ideal end-member phases. Generally, cores of elpidite euhedra are more calcic than the rims and fine-grained, late-interstitial aggregates such as shown in Figure 4B.

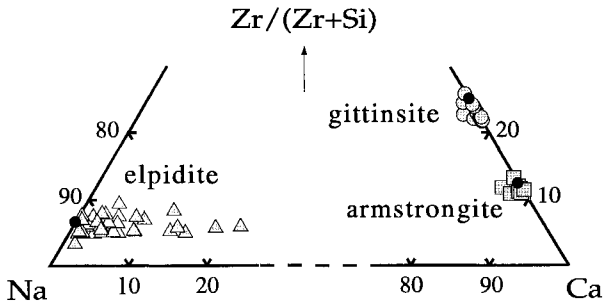


Fig. 5. Cation proportions in the Strange Lake zirconosilicate minerals calculated on the basis of seven and 15 atoms of O for anhydrous and hydrous species, respectively. Solid circles indicate end-member compositions.

### Cathodoluminescence

Elpidite, armstrongite, and gittinsite display strong luminescence when excited by an electron beam. Similar but weaker luminescence is observed under ultraviolet illumination. This property allowed the distribution of zirconosilicates to be established in many drill holes.

Cathodoluminescence observations were made using an ELM-3R Luminoscope (Herzog et al., 1970). Emission spectra were collected in the 350–850 nm wavelength range, with a grating-type H-20 Jobin-Yvon spectrometer equipped with an R-928 photomultiplier detector (Mariano and Ring, 1975).

Elpidite typically displays a greenish luminescence, which generally decays to a duller shade of blue-green after 2–3 min of continued exposure to the electron beam. To minimize this, spectra for elpidite were collected with a defocused beam, reduced power, and increased scanning interval. Emission spectra of elpidite show well-defined peaks at 425, 485, 550, and 580 nm (Fig. 6A). From comparison with spectra in Marshall (1988), we interpret the peaks at 485 and 580 nm to represent activation by $Dy^{3+}$; the 425 and 550 nm peaks are tentatively assigned to activation by $Eu^{2+}$ and $Tb^{3+}$.

Armstrongite luminesces hues of blue and does not seem to be affected by the electron-beam power density. Spectra of armstrongite are dominated by a band at about 415 nm and by a hump between 500 and 650 nm (Fig. 6B). The band at 415 nm closely resembles $Eu^{2+}$ activation in strontianite, apatite, and synthetic fluorite described by Mariano and Ring (1975). We therefore interpret $Eu^{2+}$ to be the principal activator of luminescence in armstrongite; other lanthanides may account for the hump at 500–650 nm.

Gittinsite has a distinct bright orange luminescence. This color is due to a very strong band centered at 600 nm (Fig. 6C). A wide band is also present at about 420 nm but is partially eclipsed by the 600 nm peak. Mn ion ($Mn^{2+}$) activation in apatite, feldspar, and carbonates has been shown to produce emissions between 520 and 650 nm, depending on the Mn site configuration (Marshall, 1988; Mason and Mariano, 1990). Microprobe analyses indicate that gittinsite contains up to 1.5 wt% MnO, suggesting that $Mn^{2+}$ may be the activator in this mineral. Activation at 420 nm is similar to the homologous emission in armstrongite and elpidite and is therefore attributed to $Eu^{2+}$.

## Discussion

The euhedral habit of elpidite in the equigranular granite suggests that this mineral crystallized relatively early, whereas its occurrence as interstitial anhedra in the porphyritic granite indicates relatively late-stage crystallization. In both rock types, however, elpidite is clearly a magmatic mineral and was the first zirconosilicate to form. By contrast, the textures described above show that armstrongite and gittinsite occur only as secondary subsolidus minerals, largely as replacements of elpidite.

The formation of armstrongite is readily explained by the cation-exchange reaction

$$\underset{\text{elpidite}}{Na_2ZrSi_6O_{15}\cdot 3H_2O} + Ca^{2+} = \underset{\text{armstrongite}}{CaZrSi_6O_{15}\cdot 3H_2O} + 2Na^{+}. \quad (1)$$

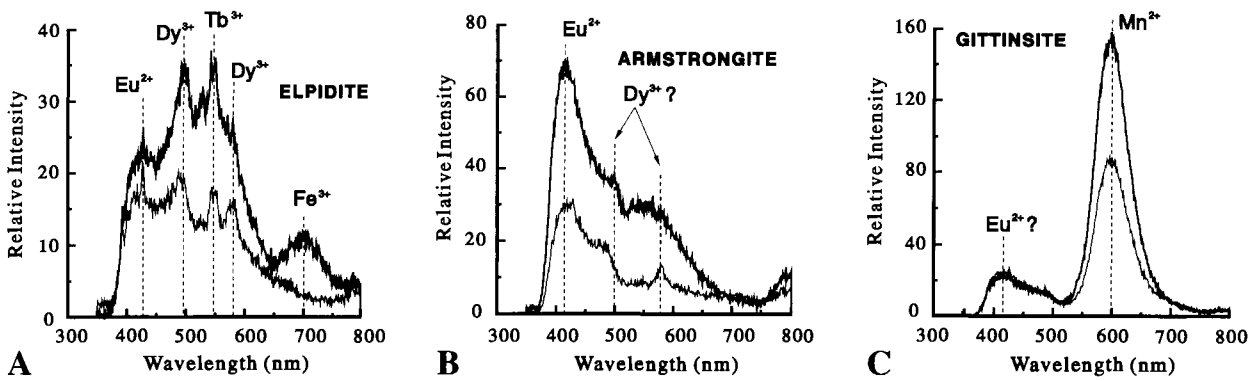


Fig. 6. Cathodoluminescence emission spectra for zirconosilicate minerals (A) elpidite, (B) armstrongite, and (C) gittinsite in subsolvus granites from Strange Lake. Beam voltage: 10–15 keV; beam current: 0.5–1 mA; beam diameter: 5 mm. Scanning at 0.5 nm increments, stepping time of 1 s. Photomultiplier high-voltage: 950 V.

This reaction has a very small negative $\Delta V_s$ (−11.01 cm³/mol; calculated from molar volume data in Marr and Wood, 1992), which corresponds to 4.8% volume reduction and is consistent with the textural evidence of essentially constant volume replacement of elpidite euhedra by armstrongite (Fig. 4D).

The replacement of elpidite by gittinsite can be explained by the reaction

$$\underset{\text{elpidite}}{Na_2ZrSi_6O_{15}\cdot 3H_2O} + Ca^{2+} + 5H_2O = \underset{\text{gittinsite}}{CaZrSi_2O_7} + 2Na^+ + 4H_4SiO_4^0. \quad (2)$$

Reaction 2 has a large negative $\Delta V_s$ (−149.1 cm³/mol or 65% volume reduction), thereby explaining the considerable porosity associated with replacement of elpidite by gittinsite in the central part of the hole (Fig. 4E and 4F). In fact, the pore volume predicted by the $\Delta V_s$ of Reaction 2 compares closely with the observed porosity created where grains of elpidite have been entirely replaced by gittinsite: 60–70%. The production of silicic acid in Reaction 2 and the absence of quartz accompanying gittinsite indicates that the altering fluid was quartz undersaturated.

In the porphyritic granite in the top 10 m of the hole, as well as in equigranular granite at shallow levels in other holes and exposed in the trench, elpidite is absent, gittinsite is the sole zirconosilicate, and there is no evidence of porosity. Instead, quartz fills the interstices around gittinsite. The similarity in the sizes and shapes of the gittinsite-quartz aggregates and the boat-shaped pseudomorphs to elpidite aggregates and euhedra in similar rocks deeper in DDH SL-182 suggest that gittinsite and quartz formed at the expense of precursor elpidite. This requires that gittinsite replacement of elpidite was accompanied or followed by precipitation of additional quartz. A reaction that might explain coprecipitation of gittinsite and quartz is

$$\underset{\text{elpidite}}{Na_2ZrSi_6O_{15}\cdot 3H_2O} + Ca^{2+} = \underset{\text{gittinsite}}{CaZrSi_2O_7} + 2Na^+ + \underset{\text{quartz}}{4SiO_2} + 3H_2O. \quad (3)$$

However, $\Delta V_s$ for this reaction is −58.4 cm³/mol. This represents a 25% volume reduction, which should be readily evident as pore space. The fact that there is no unfilled volume in the space occupied by gittinsite-quartz aggregates indicates that, if replacement was according to Reaction 3, there must have been precipitation of additional quartz. An alternative explanation, supported by preservation of delicate rosettes of gittinsite, is that replacement took place by Reaction 2 and quartz precipitated later. This implies that the metasomatic fluid was initially undersaturated with respect to quartz, and that at a later stage, silica solubility decreased thereby causing precipitation of quartz in the pores at high levels in the pluton.

The mineralogical relationships in DDH SL-182 occur throughout altered parts of the pluton and suggest that an episode of Ca metasomatism caused extensive replacement of elpidite by calcium zirconosilicates to a depth of ~70 m below the present erosional surface, and that silica was added in the form of quartz closer to the surface. On the basis of data from primary fluid inclusions in gittinsite-quartz pseudomorphs, Salvi and Williams-Jones (1990) proposed that pseudomorphism was effected by Ca-rich brines at temperatures of ~200 °C. The replacement of magmatic elpidite by gittinsite or armstrongite or both was probably caused by a similar fluid. Such low-temperature formation of gittinsite and armstrongite explains their near-end-member compositions. This contrasts with the extensive solid solution displayed by elpidite (cf. Fig. 5), which is interpreted to have crystallized under magmatic conditions; magmatic conditions for elpidite crystallization are also suggested by zoned crystals that, like plagioclase in igneous systems, were initially Ca rich. The activation of luminescence by $Eu^{2+}$ in both armstrongite and gittinsite but not elpidite (Fig. 6) is consistent with Ca metasomatism, and the fact that, in its divalent state, Eu readily substitutes for Ca.

The questions that now need to be addressed are whether the Ca metasomatism was caused by orthomagmatic fluids (Birkett et al., 1992) or externally derived formational waters (Salvi and Williams-Jones, 1990); whether or not Zr was mobilized and concentrated by the metasomatism; why armstrongite formed at depth and gittinsite closer to the surface; why quartz addition was restricted to the near-surface environment; and ultimately under what conditions and in response to what factors alteration of elpidite to armstrongite and gittinsite occurred.

The orthomagmatic fluid hypothesis can be ruled out by the evidence that the fluids responsible for the deeper alteration were quartz undersaturated. If the altering fluid were of magmatic origin it would have been in equilibrium with the granite and therefore saturated with respect to silica (any cooling would have caused deposition of quartz). Moreover, the average Ca concentration observed in altered subsolvus granite (1.5 wt% vs. 0.5 wt% in unaltered granites) cannot be explained by magmatic processes alone (cf. Nassif, 1993; Boily and Williams-Jones, 1994).

The restriction of gittinsite mainly to the volume of the precursor phase may indicate that Zr acted as an immobile element during metasomatism. However, as reported above, the proportions of gittinsite to quartz in samples from high levels are generally greater than the proportions of gittinsite to pore space lower in the hole. Although the difference is small, it could be significant because it may indicate that Zr was indeed remobilized by the metasomatic fluid, albeit to a limited degree. This would be consistent with the observed increase of whole-rock Zr in the strongly altered subsolvus granites (Fig. 2), i.e., in rocks containing the gittinsite-quartz pseudomorphs.

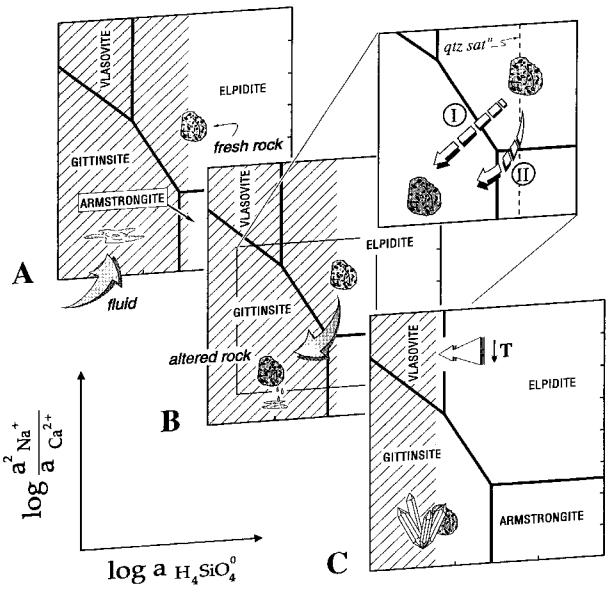


Fig. 7. Schematic log $a^2_{Na^+}/a_{Ca^{2+}}$ vs. $a_{H_4SiO_4^0}$ diagrams showing the stability fields of the zirconosilicate minerals, as well as hypothetical compositions of the unaltered elpidite-bearing granite, the hydrothermal fluid (A), and the altered gittinsite-bearing granite (C). Also shown are possible paths of metasomatic transformation of the rock during alteration (B). The shaded fields represent quartz saturation levels in the fluid during metasomatism (A and B) and at lower temperature (C).

Further insight into this metasomatic process is gained by examining the stability fields of the zirconosilicate minerals as a function of Na, Ca, and Si activity. Unfortunately, there are few thermodynamic data for the alkali and alkaline-earth zirconosilicates (cf. Marr and Wood, 1992). Nonetheless, it is possible to represent phase-stability relationships schematically using the principles of chemographic analysis (Zen, 1966). In Figure 7 we present a schematic log $a^2_{Na^+}/a_{Ca^{2+}}$ vs. log $a_{H_4SiO_4^0}$ diagram for the system $Na_2O$-CaO-$ZrO_2$-$SiO_2$-$H_2O$ and the phases in the system observed in the altered rocks of Strange Lake, plus vlasovite. Also shown on the diagram are possible locations of the boundary for quartz saturation.

We propose that, sometime after crystallization of at least the apical region of the intrusion, heated groundwaters in equilibrium with adjacent calc-silicate gneisses and gabbros (and therefore Ca-rich and quartz undersaturated) entered the pluton (Fig. 7A). In the uppermost parts where water-rock ratios were high, the fluids dissolved elpidite, replacing it primarily with gittinsite (Fig. 7B, path I). Deeper in the pluton, fluid-rock ratios were lower, permitting the rock to buffer $a_{H_4SiO_4^0}$ to higher values, which were sufficient to stabilize gittinsite plus armstrongite and locally armstrongite alone (Fig. 7B, path II).

The presence of quartz with gittinsite near the surface requires either that $P$-$T$ conditions of alteration changed so as to permit saturation of quartz at lower $a_{H_4SiO_4^0}$ or that quartz was introduced later. In view of the textures, i.e., feathery gittinsite crystals embedded in quartz, we prefer the latter explanation and propose that quartz was precipitated in response to cooling of the fluids during the waning stages of the hydrothermal system (Fig. 7C).

## Acknowledgments

The research described in this paper was supported by NSERC strategic and operating grants awarded to A.E.W.-J. and forms part of a larger project involving S. Aja, M. Boily, R. Marr, R. Martin, G. Nassif, J. Roelofsen-Ahl, and S. Wood. Additional funding was provided by FCAR (Quebec) and a NATO travel grant. We are indebted to the Iron Ore Company of Canada for allowing access to the Strange Lake property and their drill core library. The manuscript benefited from critical reviews by F. Dudas, J. Gittins, and an anonymous reviewer.

## References cited

Allan, J.F. (1992) Geology and mineralization of the Kipawa yttrium-zirconium prospect, Quebec. Exploration and Mining Geology, 1, 283–295.

Bastin, G.F., and Heijligers, H.J.M. (1991) Quantitative electron probe microanalysis of ultra-light elements (oxygen-boron). In K.F.J. Heinrich and D.E. Newbury, Eds., Electron probe quantitation, p. 145–162. Plenum, New York.

Birkett, T.C., Miller, R.R., Roberts, A.C., and Mariano, A.N. (1992) Zirconium-bearing minerals of the Strange Lake intrusive complex, Quebec-Labrador. Canadian Mineralogist, 30, 191–205.

Boily, M., and Williams-Jones, A.E. (1994) The role of magmatic and hydrothermal processes in the chemical evolution of the Strange Lake plutonic complex (Quebec-Labrador). Contributions to Mineralogy and Petrology, 118, 33–47.

Bonin, B. (1988) Peralkaline granites in Corsica: Some petrological and geochemical constraints. Rendiconti della Società Italiana di Mineralogia e Petrologia, 73, 1191–1194.

Currie, K.L. (1985) An unusual peralkaline granite near Lac Brisson, Quebec-Labrador. Geological Survey of Canada Report 85-1A, p. 73–90.

Currie, K.L., and Zaleski, E. (1985) The relative stability of elpidite and vlasovite: A $P$-$T$ indicator for peralkaline rocks. Canadian Mineralogist, 23, 577–582.

Fleet, S.G., and Cann, J.R. (1967) Vlasovite: A second occurrence and a triclinic to monoclinic inversion. Mineralogical Magazine, 36, 233–241.

Gerasimovsky, V.I. (1969) Geochemistry of the Ilímaussaq Alkaline Massif (South-West Greenland), 174 p. Nauka, Moskow (in Russian) (not seen; extracted from Lithos, 26, 167, 1990).

Goldschmidt, V. (1913) Atlas der Krystallformen, vol. 3. Carl Winters Universitätsbuchhandlung, Heidelberg, Germany.

Herzog, L.F., Marshall, D.J., and Babione, R.F. (1970) The luminoscope: A new instrument for studying the electron-stimulated luminescence of terrestrial, extra-terrestrial and synthetic materials under the microscope. In J.N. Weber and E. White, Eds., Space science applications of solid state luminescence phenomena, p. 79–98. MRL publication 70-101, State College, Pennsylvania.

Horváth, L., and Gault, R.A. (1990) The mineralogy of Mont Saint-Hilaire, Quebec. Mineralogical Record, 21, 284–359.

Kogarko, L.N. (1990) Ore-forming potential of alkaline magmas. Lithos, 26, 167–175.

Mariano, A.N., and Ring, P.J. (1975) Europium-activated cathodoluminescence in minerals. Geochimica et Cosmochimica Acta, 39, 649–660.

Marr, R.A., and Wood, S.A. (1992) Preliminary petrogenetic grids for sodium and calcium zirconosilicate minerals in felsic peralkaline rocks: The $SiO_2$-$Na_2ZrO_3$ and $SiO_2$-$CaZrO_3$ pseudobinary system. American Mineralogist, 77, 810–820.

Marshall, D.J. (1988) Cathodoluminescence of geological materials, 146 p. Unwin-Hyman, Boston.

Mason, R.A., and Mariano, A.N. (1990) Cathodoluminescence activation in manganese-bearing and rare earth-bearing synthetic calcites. Chemical Geology, 88, 191–206.

Miller, R.R. (1986) Geology of the Strange Lake Alkalic Complex and the associated Zr-Y-Be-REE mineralization. Newfoundland Department of Mines and Energy, Mineral Development Division Report 86-1, p. 11–19.

——— (1990) The Strange Like pegmatite-aplite hosted rare metal deposit, Labrador. Newfoundland Department of Mines and Energy, Geological Survey Branch, Report 90-1, p. 171–182.

Nassif, G.J. (1993) The Strange Lake peralkaline complex, Québec-Labrador: The hypersolvus-subsolvus granite transition and feldspar mineralogy, 104 p. M.Sc. thesis, McGill University, Montreal, Quebec.

Nassif, G.J., and Martin, R.F. (1991) The hypersolvus granite-subsolvus granite transition at Strange Lake, Quebec-Labrador. Geological Association of Canada Abstracts with Program, 16, A89.

Pillet, D., Bonhomme, M.G., Duthou, J.L., and Shenevoy, M. (1989) Chronologie Rb/Sr et K/Ar du granite peralkalin du lac Brisson, Labrador central, Nouveau-Québec. Canadian Journal of Earth Sciences, 26, 328–332.

Salvi, S., and Williams-Jones, A.E. (1990) The role of hydrothermal processes in the granite-hosted Zr, Y, REE deposit at Strange Lake, Quebec/Labrador: Evidence from fluid inclusions. Geochimica et Cosmochimica Acta, 54, 2403–2418.

——— (1992) Reduced orthomagmatic C-O-H-N-NaCl fluids in the Strange Lake rare-metal granitic complex, Quebec/Labrador, Canada. European Journal of Mineralogy, 4, 1155–1174.

Trueman, D.L., Pedersen, J.C., de St. Jorre, L., and Smith, D.G.W. (1988) The Thor Lake, N.W.T., rare-metal deposits. In R.P. Taylor and D.F. Strong, Eds., Granite-related mineral deposits: Geology, petrogenesis and tectonic setting. Canadian Institute of Mining and Metallurgy, Special Volume 39, 279–284.

Vlasov, K.A., Kuz'menko, M.Z., and Es'kova, E.M. (1966) The Lovozero Alkali Massif, 627 p. Oliver and Boyd, Edinburg.

Zen, E-An (1966) Construction of pressure temperature diagrams for multicomponent systems after the method of Schreinemakers: A geometrical approach. U.S. Geological Survey Bulletin, 1225, 1–56.

Manuscript received August 12, 1994
Manuscript accepted May 31, 1995